Chiral-like doublet band structure and octupole correlations in math xmlns="http://www.w3.org/1998/Math/MathML">mmultiscripts>mi>Ag/mi>mprescripts>/mprescripts>none>/none>mn>104/mn>/mmultiscripts>/math>

Kaushik Katre et al.

Phys. Rev. C **106**, 034323 — Published 27 September 2022

DOI: 10.1103/PhysRevC.106.034323

Chiral like doublet band structure and octupole correlations in ^{104}Ag

Kaushik Katre,[1,*] P. V. Madhusudhana Rao,[2] R. Raut,[3] A. Sharma,[4] K. Suryanarayana,[2] A. Tejaswi,[2] M. Ratna Raju,[2] D. Vijaya Lakshmi,[2] T. Seshi Reddy,[2] M. Kumar Raju,[5] S. Jehangir,[6] N. Rather,[6] G. H. Bhat,[7] Nazira Nazir,[7] J. A. Sheikh,[7] Y. P. Wang,[8] J. T. Matta,[9] A. D. Ayangeakaa,[10] U. Garg,[11] S. S. Ghugre,[3] T. Trivedi,[12] B. S. Naidu,[13] R. Palit,[13] S. Saha,[14] S. Muralithar,[1] and R. P. Singh[1,†]

[1] *Nuclear Physics Group, Inter-University Accelerator Centre, New Delhi 110067, India*
[2] *Department of Nuclear Physics, Andhra University, Visakhapatnam 530003, India*
[3] *UGC-DAE Consortium for Scientific Research, Kolkata Centre, Kolkata 700098, India*
[4] *Department of Physics, Himachal Pradesh University, Shimla 171005, India*
[5] *Department of Physics, GITAM School of Science, Visakhapatnam, 530045, India*
[6] *Department of Physics, Islamic University of Science and Technology, Jammu and Kashmir 192122, India*
[7] *Department of Physics, University of Kashmir, Srinagar 190006, India*
[8] *State Key Laboratory of Nuclear Physics and Technology, School of Physics, Peking University, Beijing 100871, China*
[9] *Physics Division, Oak Ridge National Laboratory, Oak Ridge, Tennessee 37831, USA*
[10] *Department of Physics and Astronomy, University of North Carolina Chapel Hill, North Carolina 27599, USA and Triangle Universities Nuclear Laboratory, Duke University, Durham, North Carolina 27708, USA*
[11] *Department of Physics and Astronomy, University of Notre Dame, Notre Dame, Indiana 46556, USA*
[12] *Department of Pure and Applied Physics, Guru Ghasidas Vishwavidyalaya, Bilaspur 495009, India*
[13] *Department of Nuclear and Atomic Physics, Tata Institute of Fundamental Research, Mumbai 400005, India*
[14] *School of Advanced Sciences, Vellore Institute of Technology, Vellore 632014, India*

(Dated: August 8, 2022)

The nature of the yrast negative-parity band and its 'chiral' like partner band in ^{104}Ag is investigated experimentally and theoretically. Lifetimes of states in the negative-parity yrast band and positive-parity band based on the 4424 keV level is measured using Doppler shift attenuation technique. Lifetime of 3 more states have been determined along with upper limit for the lifetime of the highest observed yrast states. Further, lifetime known from earlier studies are determined with better precision. The level scheme of ^{104}Ag has also been extended with the addition of new enhanced E1 transitions linking the positive-parity band based on the 4424 keV levels and the yrast negative-parity and its partner band. B(E1) and/or B(E1)/B(M1) values for the transitions from positive parity band to the yrast and its partner band have been determined for the first time; these suggest strong octupole correlation between the positive parity and the negative parity bands. Calculations based on Triaxial Projected Shell Model (TPSM) and Covariant Density Functional Theory (CDFT) have been performed to unravel the intrinsic structures of the partner band and the excited positive-parity band. TPSM calculations predict that doublet bands have significant angular momentum contributions along the three principle axis, suggesting that bands could have chiral symmetry breaking origin. The CDFT calculations predict a $\pi(g_{9/2})^{-1} \otimes \nu(h_{11/2})(g_{7/2},d_{5/2})^2$ aligned quasi-particle configuration for the negative-parity doublet bands with deformation parameters $\beta \approx 0.20$ and $\gamma \approx 5^o$. The partner band could be interpreted as a chiral vibration mode built on top of the yrast band. The excited positive-parity band is predicted to have aligned four quasi-particle configuration, namely, $\pi(g_{9/2})^{-1} \otimes \nu(h_{11/2})^2\ (g_{7/2},d_{5/2})^1$. Further, these calculations predict significant octupole softness in ^{104}Ag which could be the reason for enhanced E1 transitions between the four quasi-particle positive-parity band and the doublet negative-parity bands.

I. INTRODUCTION

The structure of nuclei in A $\sim$ 100 region exhibit single-particle and a variety of collective features. The rich band structures observed and the transitions among them render this region an ideal laboratory to test various nuclear structure models and the approximations used therein. Apart from the usual collective rotation of a deformed nucleus, many magnetic and anti-magnetic rotational (MR and AMR) bands have also been reported in nuclei in this region [1–4]. These bands are observed in nuclei near the shell closures having small deformation values. The MR bands are understood be arising from the coupling of neutron and proton angular momenta oriented almost perpendicular to each other at the band head and the generation of angular momentum is due to the alignment of these angular momenta along the rotational axis. This resembles closing of a pair of blades of a shear with neutron and proton angular momenta as the blades of the shear, thus these bands are also sometimes referred as shears band. AMR bands are interpreted to be arising due to the simultaneous alignment of two (or more) symmetric anti-aligned proton hole blades along the neu-

* k_katre@yahoo.com
† rajeshpratap07@gmail.com

tron particle angular momentum, a twin (or more) shears mechanism. Further, the phenomenon of chirality in nuclei, first suggested by Frauendorf and Meng [5] is generally accepted as one of the signatures of triaxial shapes in nuclei and it has been a major focus of recent studies in the A $\sim$ 100 region [6–9]. The phenomenon of chirality arises in nuclei due to spontaneous left-right symmetry breaking in triaxial shaped nuclei giving rise to a pair of nearly degenerate bands with identical energy states. These bands in odd-odd triaxial nuclei are thought to arise due to the alignment of angular momentum of the two odd nucleons along the long and the short axis of the nucleus for a hole and particle like nature, respectively and the angular momentum of the triaxial core aligned along the intermediate axis; thus giving rise to a left or a right-handed system in the intrinsic frame of reference, depending on which side of the short-long plane is the total angular momentum vector of the nucleus. However, states in bands of different configuration could also have accidental degeneracy, thus to qualify as true chiral bands the states in the two bands must have very similar physical properties like moment of inertia, quasi-particle alignments, in-band B(M1), B(E2) values and B(M1)/B(E2) ratios. Additionally they must also have a smooth energy staggering as a function of spin and a characteristic staggering of B(M1)/B(E2) ratios for the in-band and out of band and energy degeneracy of states at same spin [10–12].

In many cases near energy degeneracy of ‘chiral bands’ is observed but the transition probabilities in the two bands are found to be different, as in the case of ^{134}Pr [13] and ^{102}Rh [14]. In the silver isotope ^{106}Ag, chiral like bands were observed by P. Joshi *et al.* [10] based on $\pi g_{9/2}^{-1} \otimes \nu h_{11/2}$ configuration. This is the only case other than the best known candidates for chiral bands in ^{126,128}Cs [15, 16] where a crossing is observed between the chiral partners. However, Joshi *et al.* found that the bands have different shapes near the crossover point (I$\sim$14$\hbar$). These bands were further investigated by E.O. Lieder *et al.* [17] based on lifetime measurements but in conclusion they found that the yrast negative-parity band based on $\pi g_{9/2}^{-1} \otimes \nu h_{11/2}$ configuration and its proposed partner bands are not chiral partners. In fact, they suggested a different configuration, discussed in detail in the present work, to the partner band. Wang *et al.* [18] reported observation of chiral doublet bands based on $\pi g_{9/2}^{-1} \otimes \nu h_{11/2}$ configuration in ^{104}Ag, however, earlier study by Datta *et al.* [19] had found these bands to be magnetic rotational bands. Dar *et al.* [20] analysed such doublet bands in A $\sim$ 100 (including such bands in ^{106,104}Ag) based on Triaxial Projected Shell Model (TPSM) and concluded that these bands have different intrinsic structures. Further, few relatively strong E1 transitions were observed from a positive-parity band with band head at 4424 keV and the yrast negative-parity band. The positive-parity band was suggested to have a four quasi-particle $\pi(g_{9/2})^{-1} \otimes \nu\,(h_{11/2})^2(g_{7/2},d_{5/2})$ configuration in Ref. [18, 19]. In an effort to have a better understanding of the underlying intrinsic structures and interactions between the bands, lifetime measurements of the levels in the yrast and the excited bands were performed in the present work. In section II, the details of the experiment are described; section III gives the details of analysis and results including the observation some new interband and intraband γ-transitions, in section IV the results are discussed using the TPSM and Covariant Density Functional Theory (CDFT); and finally section V summarizes the present work.

II. EXPERIMENTAL DETAILS

High spin excited states of ^{104}Ag nucleus were populated by using ^{76}Ge (^{32}S, p3nγ)^{104}Ag fusion evaporation reaction at beam energy of 110 MeV. The ^{32}S beam was delivered by 14-UD BARC-TIFR Pelletron Facility at Tata Institute of Fundamental Research (TIFR), Mumbai. The target was fabricated by evaporating enriched ^{76}Ge (500 µg/cm^2) on gold foil of thickness 26 mg/cm^2. A thin layer of aluminium (11 µg/cm^2) acted as adhesive was placed between ^{76}Ge and gold foil. The emitted de-exciting gamma rays were detected by Indian National Gamma Array (INGA) consisting of 18 Compton suppressed clover detectors [21]. The clover detectors were placed at 6 different angles viz. 40°, 65°, 90°, 115°, 140° and 157° with respect to the beam direction. Approximately 3.2 x 10^9 two and higher-fold $\gamma-\gamma$ coincidence event collected. The energy and efficiency calibration were done by using standard ^{152}Eu and ^{133}Ba radioactive sources placed at the target position.

III. DATA ANALYSIS AND RESULTS

A. Level Scheme

The data were sorted in γ-γ symmetric and asymmetric matrices by using MARCOS program [21] and analysed using RADWARE software packages [22, 23]. The symmetric matrix was used to check the published level scheme and to place new gamma rays in the level scheme by generating various gated spectra and asymmetric matrix were used to determine the multipolarities of the γ-ray transitions from the measurement of the ratio of directional correlation from oriented states (R$_{DCO}$) [24]. The asymmetric matrix with gamma rays detected by detectors at 140° ring on one axis and gamma rays detected by detectors at 90° on other axis was used to determine DCO ratios and defined as

$$R_{DCO} = \frac{I_\gamma \text{ (Observed at } 140^\circ \text{ , gate on } 90^\circ)}{I_\gamma \text{ (Observed at } 90^\circ\text{, gate on } 140^\circ)}$$

The DCO ratios determined for most of the transitions are by using 346 keV ($10^- \rightarrow 9^-$) γ-ray as gate, the typical value of DCO ratio for a quadrupole transition was found to be ~ 1.6 and for a dipole transition it was ~ 1.0. The DCO ratios determined were found consistent with earlier study by P. Datta *et al.* [19].

The partial level scheme of the odd-odd ^{104}Ag nucleus obtained from present work is shown in Fig. 1. In Fig. 2(a) gated gamma ray spectra are shown with gate on 865 keV ($8^{-}\rightarrow 7^{+}$, band A), 406 keV ($17^{+} \rightarrow 16^{+}$, band C) γ-ray in 2(b) and with gate on 450 keV ($15^{-}\rightarrow 14^{-}$, band B) γ-ray in 2(c). The level scheme was built on the basis of coincidence relationship, relative intensities and directional correlation of gamma rays. Most of the γ-transitions reported in the earlier studies [[18], [19]] were observed, however, transitions only relevant to the present study are shown in partial level scheme in Fig. 1 as listed in Table I. Four new gamma transitions 947 keV, 1069 keV, 607 keV and 747 keV were also observed and placed in the level scheme. The details of gamma energies, level energies, initial and final spin states, R_{DCO} are given in Table I. In the previous study by Z. Wang *et al.* [18] the placement of 1232.6 keV γ-ray transition, de-exciting 6133 keV level in the yrast band was tentative. In the present study, the placement and spin of 19$\hbar$ for the 6133 keV level based on coincidence conditions and DCO ratio measurements of 605 keV transition are confirmed. The negative-parity for 6133 keV level is because 1233 keV transition could only be E2 since M2 or other higher multipolarities are much less likely. Therefore, for this level spin-parity adopted is 19^{-}.

In band B, the R_{DCO} values of 499 keV and 329 keV transitions de-exciting from 2711 keV and 3040 keV levels, respectively, are found to be close to 1 with a gate on a dipole 175 keV transition with very little mixing [19, 25] thus, the spin assignments of levels 2711 and 3040 keV levels are confirmed, however, parities are still kept tentative following the adoption by Z. Wang *et al.* [18]. A new transition (607 keV) de-exciting from level at 3648 keV to level at 3040 keV was observed and is placed in the level scheme. Two new E1 transitions from band C to band B from 17^{+} to 16^{-} (947 keV) and from 16^{+} to 15^{-} (1069 keV) were also observed and are placed in the level scheme. These new transitions can be seen in Fig. 2(c) in the gated spectra with gate on 450 keV ($15^{-}\rightarrow 14^{-}$) transition in band B with E_{γ} marked in red colour. Other gated γ-spectra are also shown in Fig. 2(a) and (b).

B. Level Lifetime Analysis using the Doppler Shift Attenuation Method (DSAM)

DSAM analysis was carried out to extract lifetime of excited states of band A and band C. Data were sorted into angle dependent asymmetric matrices, wherein the γ-rays observed at one of the four (40°, 65°, 140° and 157°) possible angles on the y-axis and coincident γ-rays detected at the 90° on the x-axis. The analysis was carried out by using the LINESHAPE [26] package together with developments reported in the Ref. [27]. The same is merited with the use of stopping powers of SRIM [28] software for simulation of residue trajectories through target and backing media and thus reduces systematic uncertainty on the lifetime results vis-a-vis that from the use of older stopping power models as implemented in the LINESHAPE package. As per the routine procedure of the DSAM analysis, the calculated Doppler-broadened lineshapes were least square fitted to the experimental spectra at different angles in order to determine the lifetime of the respective level. The detailed methodology is described in a number of papers such as Ref. [29]. The parameters of fitting include the level lifetime, the side feeding lifetime, the spectrum background and the height of the transition peak along with that of the neighbouring contamination peak, if any. For each level of interest, a single feeder state was used to model the side feeding contribution to the observed experimental γ-ray transition peak. During the analysis χ^2 minimization was carried out for experimental spectra beginning from the topmost level which was assumed to be 100% side fed. Lifetime of the level, the side feeding time and other parameter were allowed to vary for converging into a χ^2 minimum. In the second step, the side feeding time and the lifetime of levels were allowed to vary simultaneously while keeping the other (spectrum) parameters of individual states fixed at the values obtained in the previous steps. The lifetimes corresponding to those arrived at from this global minimization were the final values quoted herein.

In the present DSAM analysis both spectra generated with gate on transition below (GTB) as well as spectra with gate on transition above (GTA) the transition of interest wherever feasible, are used. One of the spectra corresponding to the GTB was generated by summing gates on 346 keV, 333 keV and 444 keV transitions of the yrast band (Band A). Lifetimes of the states 15^{-}, 16^{-}, 17^{-}, 18^{-} and 19^{-} belonging to Band A, were extracted from analysis of this spectrum. The experimental spectra along with fitted Doppler shapes at four different angles for some of these de-exciting transitions are shown in Fig. 3 (a,b). Lifetimes of the 16^{+} and the 17^{+} states of band C were also extracted from analysis of the same spectrum with GTB.

As far as the present data are concerned, no Doppler shapes were observed for transition de-exciting the 14^{+} and the 15^{+} states of Band C. Given the stopping time of the ^{104}Ag residues in the target and backing media for the experiment is ~ 1.3 ps, not observing Doppler shape for these transitions would mean that the lifetimes of the corresponding levels are > 4 ps. This is consistent with the propositions of Datta *et al.* [19]. The lifetime of the 16^{+} and 17^{+} states, as mentioned earlier, could be determined from the analysis of the GTB spectrum corresponding to the sum gates on 346 keV, 333 keV and 444 keV keV transitions of Band A. The lifetimes of the still higher (18^{+}, 19^{+}) states of Band C were extracted from analysis of another GTB spectrum generated from the sum of gates on 361 keV , 1604 keV, 1484 keV, 926 keV and

TABLE I. γ energy (E_γ), level energy (E_i), relative intensity (I_γ), R_{DCO} of the γ transitions in ^{104}Ag obtain from the gate on pure dipole 346 keV transition.

E_γ(keV)*	E_i(keV)	$J_i^\pi \to J_j^\pi$	Intensity(I_γ)	DCO ratio(R_{DCO})
99.3	212	$7^+ \to 6^+$	120.6(60)	
112.6	113	$6^+ \to 5^+$	162.9(81)	
175.2	1253	$9^- \to 8^-$	126.0(63)	0.95(1)
297.2	3648	$14^- \to 13^-$	5.1(3)	1.06(8)
310.1	3351	$13^- \to 12^-$	3.7(2)	1.06(11)
328.9	3040	$12^- \to 11^{(-)}$	1.7(1)	1.07(11)[a]
332.8	1932	$11^- \to 10^-$	89.6(45)	1.01(3)
346.3	1599	$10^- \to 9^-$	100.0(50)	1.13(1)[b]
361.4	4786	$15^+ \to 14^+$	2.9(2)	0.91(9)
380.8	5166	$16^+ \to 15^+$	7.3(4)	0.99(12)
406.1	5572	$17^+ \to 16^+$	9.9(5)	0.92(5)
443.8	2376	$12^- \to 11^-$	53.9(52)	0.99(1)
444.7	2820	$13^- \to 12^-$	50.9(25)	0.99(1)
449.6	4097	$15^- \to 14^-$	5.8(3)	0.90(7)
480.1	6053	$18^+ \to 17^+$	10.5(5)	
481.2	3301	$14^- \to 13^-$	40.3(20)	1.02(2)
499.3	2711	$11^{(-)} \to 10^{(-)}$	1.6(3)	1.02(14)[a]
507.8	3809	$15^- \to 14^-$	26.4(13)	0.93(2)
519.8	4329	$16^- \to 15^-$	15.6(8)	0.90(5)
521.7	1599	$10^- \to 8^-$	3.7(2)	
527.6	4625	$16^- \to 15^-$	4.8(2)	1.08(11)
543.6	6596	$19^+ \to 18^+$	2.9(2)	
564.2	7161	$20^+ \to 19^+$	2.7(2)	
572.3	4901	$17^- \to 16^-$	7.9(4)	0.90(6)
604.8	6133	$19^- \to 18^-$	4.8(3)	0.91(9)
606.6	3648	$14^- \to 12^-$	0.6(2)	
627.7	5529	$18^- \to 17^-$	5.5(3)	1.00(13)
638.9	3351	$13^- \to 11^{(-)}$	0.7(1)	
678.9	1932	$11^- \to 9^-$	17.4(9)	1.55(3)[b]
746.7	4097	$15^- \to 13^-$	$\leq$1	
776.7	2376	$12^- \to 10^-$	12.3(6)	1.64(8)
796.2	4097	$15^- \to 14^-$	0.7(1)	
827.7	3040	$12^- \to 10^{(-)}$	0.8(2)	
828.1	3648	$14^- \to 13^-$	3.4(2)	1.13(8)
865.2	1077	$8^- \to 7^+$	40.6(21)#	
888.4	2820	$13^- \to 11^-$	15.5(8)	1.56(13)
925.8	3301	$14^- \to 12^-$	11.2(6)	1.49(14)
946.9	5572	$17^+ \to 16^-$	1.0(1)	
959.3	2212	$10^{(-)} \to 9^-$	2.4(2)	
975.3	3351	$13^- \to 12^-$	2.6(2)	1.03(18)
977.1	4625	$16^- \to 14^-$	1.0(2)	
989.0	3809	$15^- \to 13^-$	7.6(4)	1.40(7)
1027.3	4329	$16^- \to 14^-$	4.9(3)	
1069.4	5166	$16^+ \to 15^-$	1.0(1)	
1091.8	4901	$17^- \to 15^-$	2.2(1)	
1108.9	3040	$12^- \to 11^-$	3.3(2)	1.09(10)
1112.9	2711	$11^{(-)} \to 10^-$	1.5(1)	
1200.1	5529	$18^- \to 16^-$	2.1(3)	
1232.6	6133	$19^- \to 17^-$	1.8(3)	
1357.4	5166	$16^+ \to 15^-$	3.1(2)	1.10(33)
1399.3	5208	$\to 15^-$	1.1(1)	
1484.4	4786	$15^+ \to 14^-$	5.2(3)	0.88(12)
1604.4	4424	$14^+ \to 13^-$	3.0(2)	1.04(25)

[a]DCO ratio from gate on 175 keV dipole transition

[b]DCO ratio from gate on 444 keV dipole transition

* The uncertainty in γ-ray energy is within 0.5 keV and the level energies are rounded of to the nearest integer value.

The level at 1077 keV de-excites by other transitions to lower levels as reported in [18], these were observed in the present study but not listed in this table.

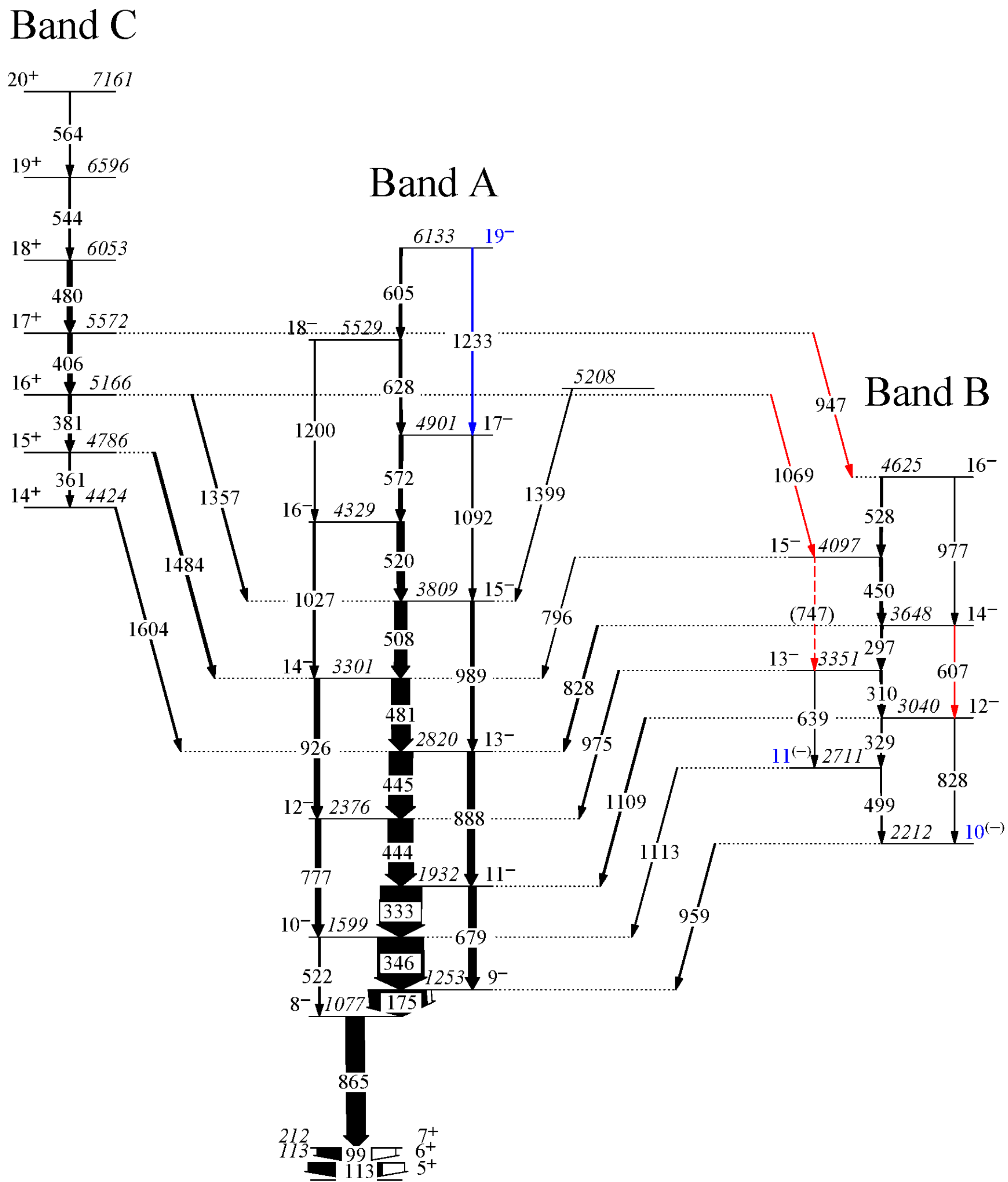

FIG. 1. Partial level scheme of the ^{104}Ag nucleus obtained from the present work, only γ-ray transitions relevant to the present study are shown, see text for details. The newly added γ-ray transitions are shown in red colour and the confirmed γ-ray transitions or spin/parity are shown in blue colour. The widths of the arrow correspond approximately to the intensity of the γ-ray transition.

989 keV transitions. The choice of gates was such that there was no contribution of the 481 keV ($14^- \to 13^-$) transition in the observed Doppler shape of the 480 keV ($18^+ \to 17^+$) transition peak of Band C. That, because in this selection of gates, the 481 keV transition of Band A is being contributed only by the 1484 keV transition de-exciting the long-lived 15^+ state of Band C. Thus, the 481 keV transition peak could be defined as a stopped contaminant one in the analysis of the Doppler shape of the 480 keV transition.

The B(E1)/B(M1) and B(E1) values determined for transitions from Band C to Band A and Band B are given in Table III.

Lifetimes of some of the states of Band A could also be determined from analysis of spectrum corresponding to a gate set on transition above (GTA) the levels of interest. Such analysis is known to eliminate the uncertainties associated with the sidefeeding, albeit the count statistics in the (GTA) spectra is often sparse and the technique cannot be practiced at large. In the present analysis, a gate on the 572 keV ($17^- \to 16^-$) was used to determine the lifetimes of the 14^-, 15^-, 16^- levels of Band A, that

TABLE II. Spin (I^{π}), γ-energy (E_{γ}), level energy, measured level lifetime from present work using the GTB (τ_{GTB}), side feeding lifetime obtain from GTB technique ($\tau_{S.F.}$) and level lifetime obtain using GTA (τ_{GTA}) technique, Adopted lifetime (τ), the reduced transition probabilities B(M1) for band A and band C.

I^{π} ($\hbar$)	E_{γ} (keV)	Level energy (keV)	τ_{GTB} (ps)	$\tau_{S.F.}$ (ps)	τ_{GTA} (ps)	Adopted τ (ps)	B(M1)↓ μ_N^2	B(M1)↓ (W.u.)
Band A								
14^-	481.2	3301			$0.52^{+0.06}_{-0.06}$	$0.52^{+0.06}_{-0.06}$	$0.76^{+0.09}_{-0.09}$	$0.42^{+0.05}_{-0.05}$
15^-	507.8	3809	$0.37^{+0.05}_{-0.05}$	$0.43^{+0.05}_{-0.05}$	$0.40^{+0.06}_{-0.05}$	$0.40^{+0.06}_{-0.05}$	$0.85^{+0.13}_{-0.11}$	$0.47^{+0.07}_{-0.06}$
16^-	519.8	4329	$0.37^{+0.05}_{-0.05}$	$0.35^{+0.05}_{-0.05}$	$0.37^{+0.06}_{-0.06}$	$0.37^{+0.06}_{-0.05}$	$0.83^{+0.13}_{-0.11}$	$0.46^{+0.07}_{-0.06}$
17^-	572.3	4901	$0.25^{+0.05}_{-0.05}$	$0.31^{+0.06}_{-0.05}$		$0.25^{+0.05}_{-0.05}$	$0.95^{+0.19}_{-0.19}$	$0.53^{+0.11}_{-0.11}$
18^-	627.7	5529	$0.29^{+0.05}_{-0.05}$	$0.19^{+0.08}_{-0.05}$		$0.29^{+0.05}_{-0.05}$	$0.58^{+0.10}_{-0.10}$	$0.32^{+0.06}_{-0.06}$
19^-	604.8	6133	0.68 ↓			0.68 ↓	0.28 ↑	0.16 ↑
Band C								
16^+	380.8	5166	$0.61^{+0.05}_{-0.05}$	$0.79^{+0.06}_{-0.06}$		$0.61^{+0.05}_{-0.05}$	$1.08^{+0.09}_{-0.09}$	$0.60^{+0.05}_{-0.05}$
17^+	406.1	5572	1.34 ↓			1.34 ↓	0.58 ↑	0.32 ↑
18^+	480.1	6053	$0.39^{+0.05}_{-0.05}$	$0.41^{+0.05}_{-0.05}$		$0.39^{+0.05}_{-0.05}$	$1.31^{+0.17}_{-0.17}$	$0.73^{+0.09}_{-0.09}$
19^+	543.6	6596	0.86 ↓			0.86 ↓	0.41 ↑	0.23 ↑

TABLE III. Spin (I^{π}), γ-energy (E_{γ}), branching ratio, B(E1)/B(M1) values, the reduced transition probabilities B(E1).

I^{π} ($\hbar$)	E_{γ}(E1) (MeV)	Br.	B(E1)/B(M1) $(10^{-4}\ \mathrm{efm}/\mu_N)^2$	B(E1)↓ (10^{-5} W.u.)
15^+	1.484	0.64	$2.84^{+0.25}_{-0.25}$	
16^+	1.357	0.27	$1.03^{+0.09}_{-0.09}$	$7.84^{+0.64}_{-0.64}$
	1.069	0.09	$0.68^{+0.08}_{-0.08}$	$5.34^{+0.44}_{-0.44}$
17^+	0.947	0.09	$0.88^{+0.10}_{-0.10}$	3.50 ↑

are respectively de-excited by the 481 keV, 508 keV and 520 keV transitions. The fitted lineshapes to the experimental spectra at four different angles for 481 keV de-exciting transition is shown in Fig. 3 (c). The extracted lifetimes of 14^-, 15^-, 16^- states has been tabulated in Table II. The lifetime values obtained for the 15^- and 16^- states are in superior overlap with these obtained from the previous analysis using spectrum corresponding to the GTB. This provides a validation for the latter. The uncertainties on lifetime values have been calculated from χ^2 analysis added in quadrature to the systematic contribution of the stopping powers that is $\sim 5\%$ [28] .

The reduced transitional probability was calculated from the measured level lifetime τ, using [30]

$$B(M1)\downarrow = \frac{0.05697 B_{\gamma}(M1)}{E_{\gamma}^3(M1)\tau[1+\alpha_t(M1)]}[(\mu_N)^2] \qquad (1)$$

where $\alpha_t(M1)$ is the total internal conversion coefficient of the transition and $B_{\gamma}(M1)$ is the branching ratio. The E_{γ} in the above expression is in MeV and τ is in picosecond. We have assumed the values of mixing ratio to be negligible to estimate the B(M1) values. Further, for $E_{\gamma} > 300$ keV the total internal conversion coefficient of the transition $\alpha_t(M1)$ is found to be negligible.

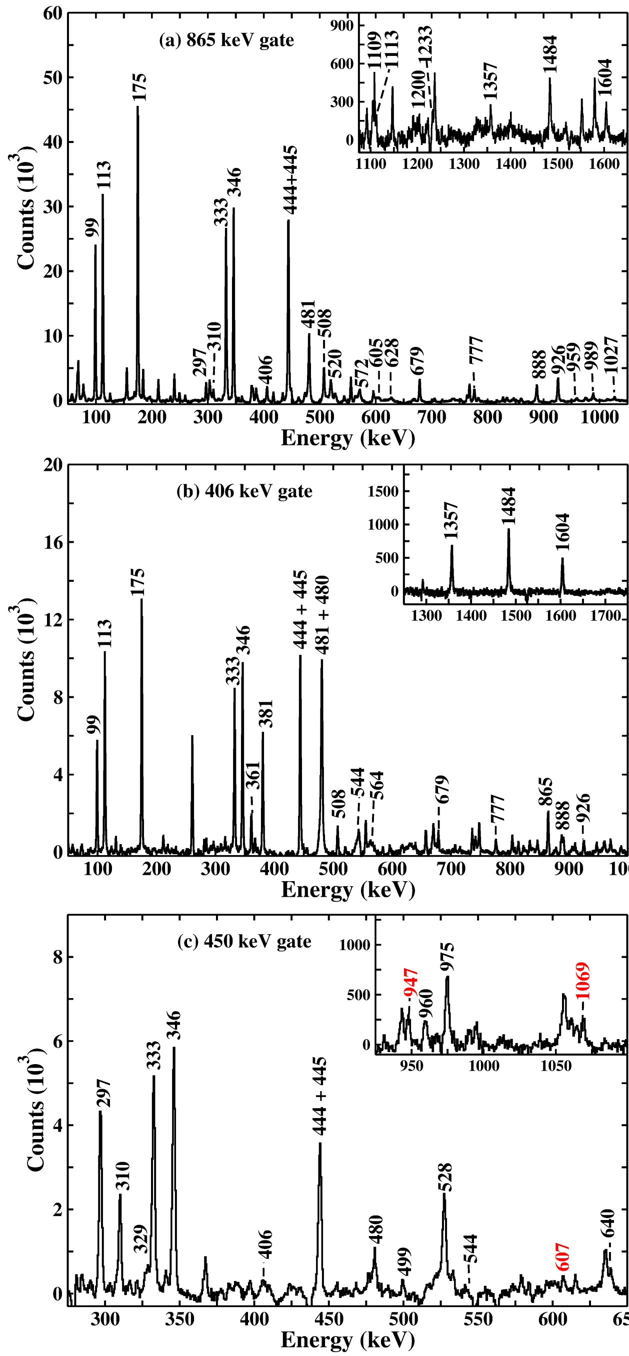

FIG. 2. γ-γ coincidence spectra with the (a) 865 keV, (b) 406 keV and (c) 450 keV gates belonging to Band A, Band C and Band B respectively. The newly observed γ transition from the present work are shown with energy marking in red colour.

IV. DISCUSSION

In the study by P. Datta *et al.* [19] the yrast Band A and Band B (Fig.1) were assigned $\pi(g_{9/2})^{-1}$ $\otimes$ $\nu(h_{11/2})(g_{7/2},d_{5/2})^2$ configuration with the neutron quasiparticle in favoured and unfavoured orbits of $h_{11/2}$ orbital respectively based on cranked shell model calculations. These bands were further proposed to be magnetic rotational bands. Wang *et al.* [18] claimed that Band A and Band B were chiral partner bands based on $\pi(g_{9/2})^{-1} \otimes \nu(h_{11/2})$ configuration, however, it was also stated that more experimental data were required to confirm this conclusion. The positive-parity Band C was also assigned to be a magnetic rotational band in Ref. [19] using tilted axis cranking calculations and in Ref. [18] this band was assigned a four quasiparticle configuration: $\pi(g_{9/2})^{-1} \otimes \nu(h_{11/2})^2(g_{7/2},d_{5/2})^1$ based on comparison to four quasiparticle bands in neighbouring ^{106}Ag [31] and ^{108}Ag [32] silver isotopes.

The E1 transitions from the positive-parity Band C to the negative-parity bands are significantly strong as is evident from Table III with high B(E1) values ($\sim10^{-4}$ W.u.). In ^{109}Te, De Angelis *et al.* [33] had reported strong E1 transitions with similar B(E1) values between bands with $(h_{11/2})^2(g_{7/2},d_{5/2})^1$ and $(h_{11/2})(g_{7/2},d_{5/2})^2$ configurations in ^{109}Te. These were ascribed to strong octupole correlations due to the mixing of configurations induced by rotation. It is to be noted that such strong octupole correlations have been observed in ^{108}Te [34], ^{114}Xe [35], ^{117}Xe [36] and ^{124,125}Cs [37] nuclei close to A$\sim$100 region similar to those reported in ^{124,125}Ba [38].

To better understand the above band structures and the measured transition probabilities, we have carried out Triaxial Projected Shell Model (TPSM) and Covarient Density Functional Theory (CDFT) calculations. Predictions of these models and their comparison with the data are described below:

A. Triaxial Projected Shell Model Results

In recent years, the TPSM approach has been demonstrated to reproduce the high-spin properties of well deformed and transitional nuclei reasonably well [39, 40]. In particular, it has been shown that it reproduces the properties of doublet bands observed in odd-odd [41], odd-mass [42] and also in even-even [39] systems quite well. In the earlier version, the basis space in the TPSM approach for odd-odd nuclei was composed of one-neutron coupled to one-proton quasiparticle configurations [43]. This basis space was obviously quite restrictive and allowed to study only low-lying states in odd-odd nuclei. To study the high-spin states in odd-odd nuclei around and beyond the band crossing, it is important to include two-neutron and two-proton states coupled to the basic one-neutron plus one-proton state. These basis states have been recently included in the TPSM approach and already some studies have been performed [41]. In order to investigate the properties of ^{104}Ag, the TPSM basis states have been constructed with the basis deformation of $\epsilon = 0.142$ and $\epsilon' = 0.100$, which correspond to quadrupole deformation $\beta\sim0.15$ and $\gamma\sim35^o$ [19, 44]. The deformed triaxial basis generated are projected onto good angular-momentum states through

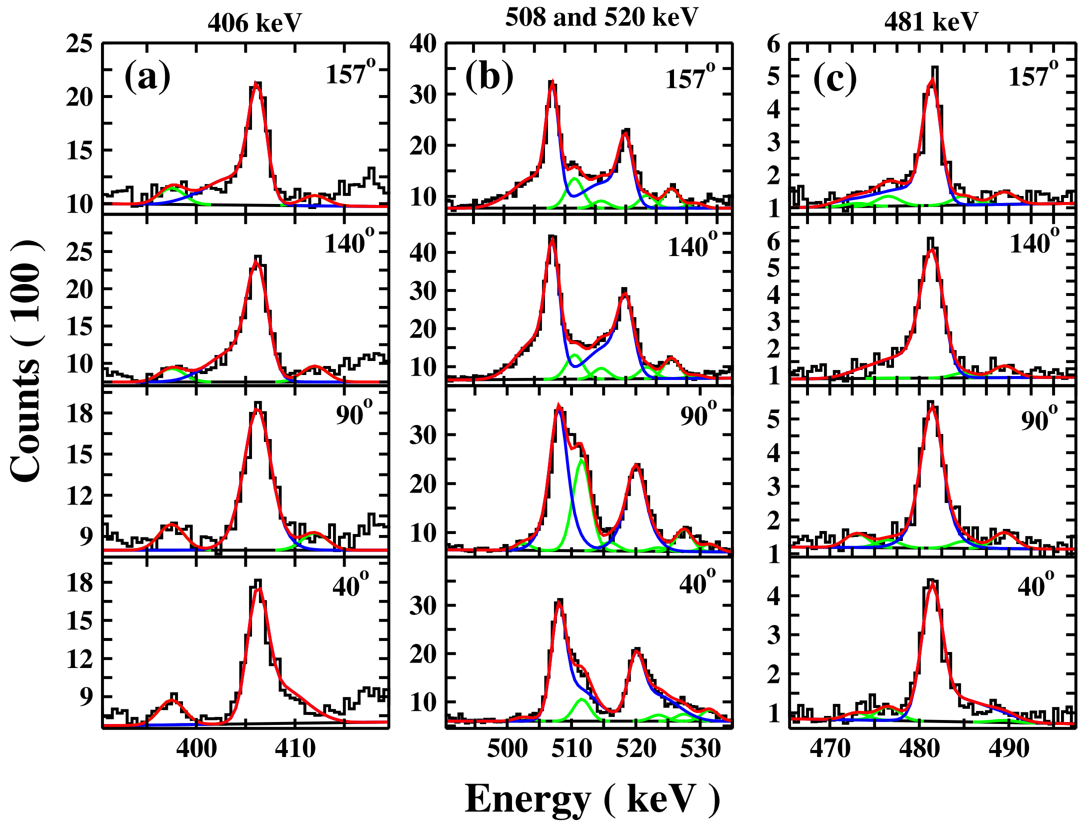

FIG. 3. The experimental spectra along with the fitted lineshape for the γ transitions 406 keV, 508 keV, 520 keV and 481 keV transition of band A and C. The lineshape of the γ transition, contamination peaks and total lineshape are shown by blue, green and red curves, respectively.

three-dimensional angular-momentum projection formalism [45]. The projected basis are then employed to diagonalize the shell model Hamiltonian consisting of pairing plus quadrupole-quadrupole interaction terms. The projected energies obtained after shell model diagonalization for ^{104}Ag odd-odd nucleus are depicted and compared with the corresponding experimental data in Fig. 4. It is evident from the figure that overall agreement between the calculated and the measured energies is quite reasonable.

In order to shed light on the possibility that two observed negative bands may be associated with the chiral symmetry breaking mechanism, we have calculated the angular momentum projections along the three principle axis. As is well known that chiral symmetry results for a triaxial system, having finite angular-momentum projection along all the three principle axis. The angular-momentum projections are plotted in Fig. 5 for the two doublet bands, and it is evident from the results that three axis have finite angular-momentum projections. This suggests that two negative-parity observed bands could be associated with the chiral symmetry. Similar analysis have recently been carried out for ^{104}Mo in ref. [48], and more details on the calculations can be found in the cited article.

In Fig. 6 the experimental kinematic moment of in-

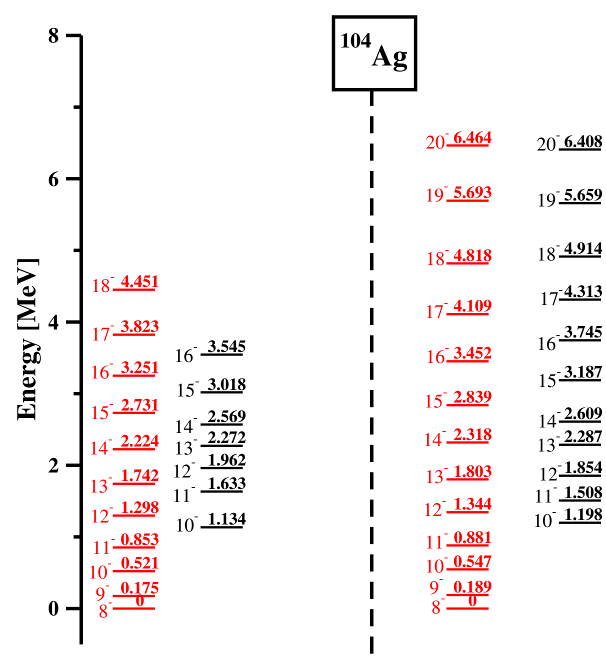

FIG. 4. Comparison of the measured energy levels of negative-parity yrast and excited bands for ^{104}Ag nucleus (left side) with that of the results of TPSM calculation (right side).

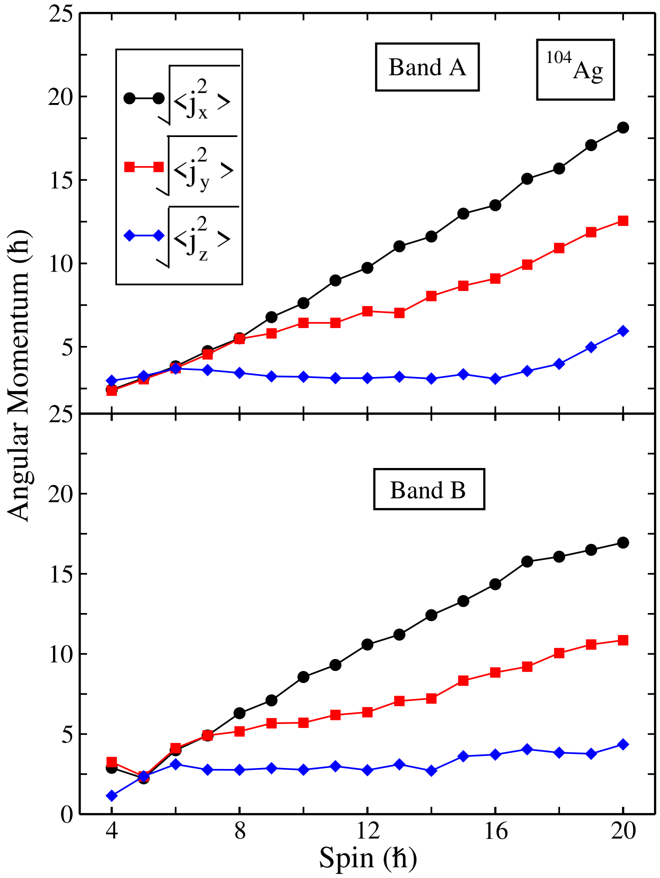

FIG. 5. The expectation values of the squared angular momentum components in band A and band B for the nucleus ^{104}Ag.

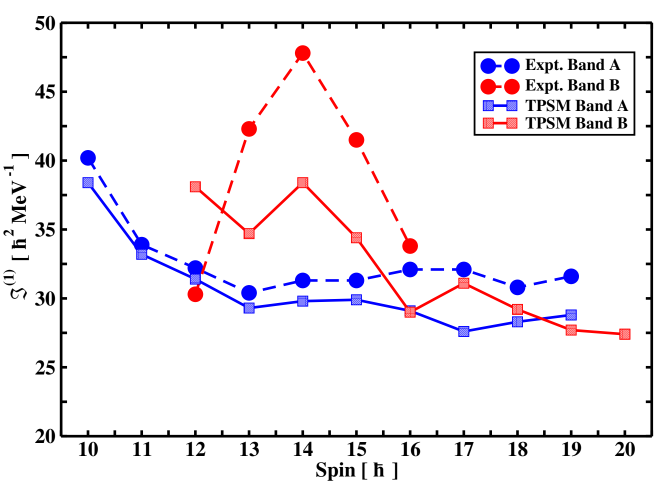

FIG. 6. Comparison between experimental and calculated moment of inertia, $J^{(1)}$ of the yrast band and partner band for ^{104}Ag. The Harries parameters used are $\Im_0$=7.0 $\hbar^2$/MeV, $\Im_1$=15.0 $\hbar^4$/MeV [46].

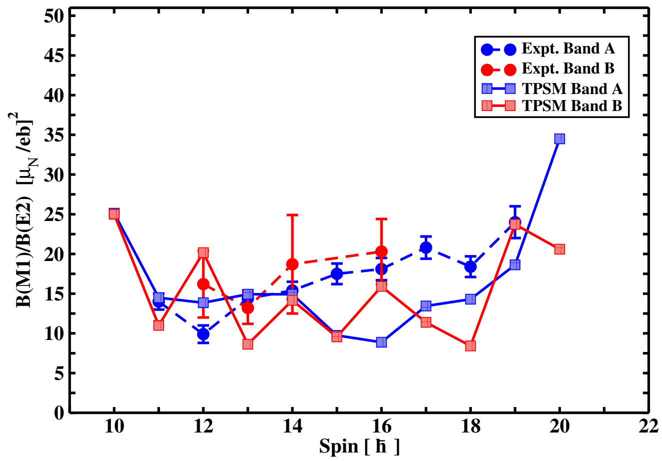

FIG. 7. Comparison of the experimental and theoretical B(M1)/B(E2) ratios for ^{104}Ag.

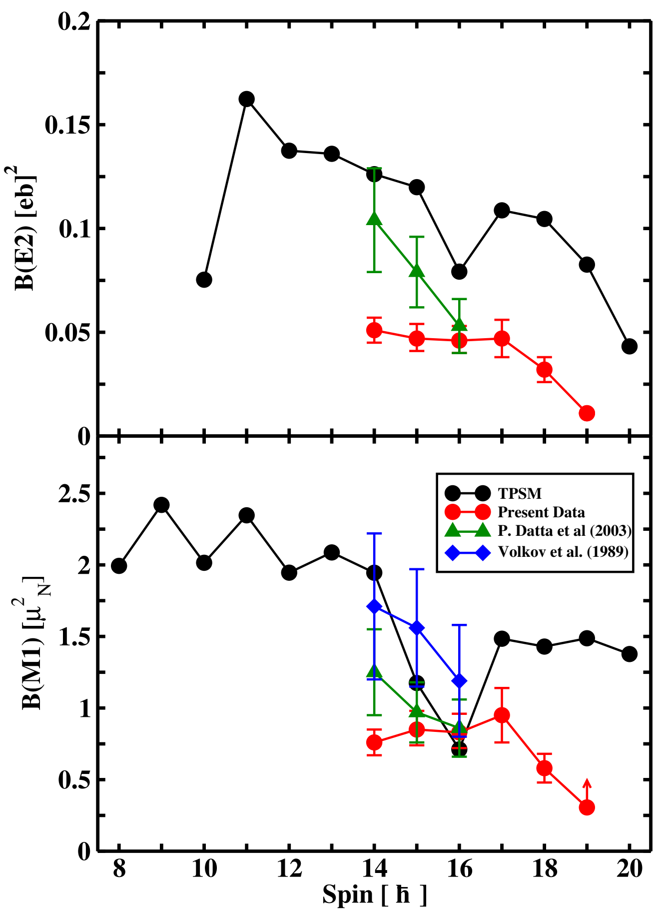

FIG. 8. Comparison of the experimental and theoretical B(M1) and B(E2) for Band A of ^{104}Ag nucleus. The error depicted for the present study include error in stopping power $\sim 5\%$ (The error bars shown for data points from the previous studies [19, 47] does not include the stopping power error)

ertia is compared with the calculated moment of inertia for bands A and B. The moment of inertia for the two bands are quite different at spins below $15\hbar$, however they tend to become similar at higher spins. The transition probabilities have also been evaluated using the projected wave functions after diagonalization with the expressions given in Ref. [43]. The parameters of $g_l^\pi = 1,\ g_l^\nu = 0,\ g_s^\pi = 5.586 \times 0.85,\ g_s^\nu = -3.826 \times 0.85$ and the effective charges of $e^\pi = 1.5e$ and $e^\nu = 0.5e$ have been employed as in our earlier work [43].It is evident from Fig.7 that B(M1)/B(E2) ratios of the yrast and the partner band are in good agreement with the experimental data. The calculated transition probabilities B(M1) and B(E2) versus spin are compared with the experimental data in Fig. 8. Individual calculated values are compared with the known values from various experimental measurements. The TPSM calculated B(E2) values are slightly higher than the measured ones. To investigate positive-parity states in ^{104}Ag, TPSM approach needs to be generalised to include two major shells for the valence space. This development is presently under progress and the results will be published in a separate communication.

B. Covariant Density Functional Theory Results

To understand the structure of the bands in ^{104}Ag, calculations based on the covariant density functional theory (CDFT) [49–51] have been carried out. The energy spectra, angular momenta and electromagnetic transition probabilities have been calculated by the three-dimensional cranking covariant density functional theory (3DTAC-CDFT) [52–54]. The octupole deformation of the ground state in ^{104}Ag has been examined based on CDFT in 3D lattice [55–57]. The relativistic density functional PC-PK1 [58] is used, which has demonstrated high predictive power to describe nuclear masses [59–61], magnetic and antimagnetic rotations [62–64] and chiral rotations [52], etc. For the 3DTAC-CDFT calculation, the Dirac equation is solved in a 3D harmonic oscillator basis in Cartesian coordinates with 10 major shells which provide convergent results for nuclei in $A \sim 100$ mass region [52]. The configuration-fixed constrained triaxial CDFT calculations similar to those in Ref. [65] were performed for various low-lying particle-hole excitations in ^{104}Ag. Detailed results are listed in Table. IV. Three positive-parity configurations are labelled as $\alpha+$, $\beta+$ and $\gamma+$. Two negative-parity configurations are labeled as $\alpha-$ and $\beta-$.

The energy spectra based on these configurations are shown in Fig. 9 in comparison with the experimental data. For the negative-parity band A, the configuration $\beta-$ can be excluded because its energy is too high. The possible configuration is $\alpha-$. At the rotational frequency $\hbar\omega = 0.0$ MeV, the alignment of the valence neutrons in $(g_{7/2}, d_{5/2})$ orbits of $\alpha-$ is roughly zero, indicating they are fully paired. As the rotational frequency increases,

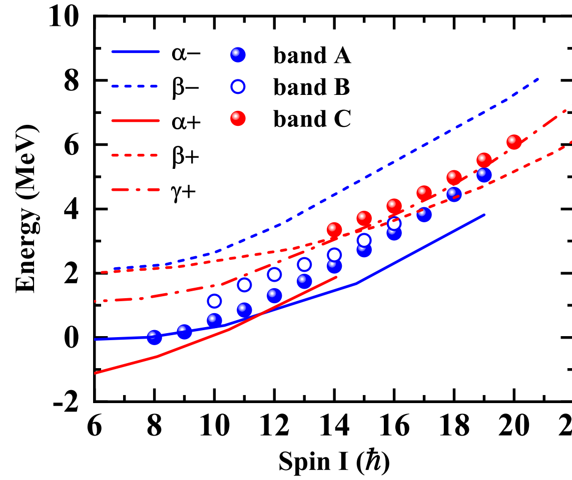

FIG. 9. Calculated rotational energies as function of the angular momenta in comparison with the data.

two of the valence neutrons in $(g_{7/2}, d_{5/2})$ orbits align toward each other and contribute an angular momentum of roughly $6\hbar$ at the rotational frequency $\hbar\omega = 0.4$ MeV (I$\sim 12\hbar$). There is no proper configuration for band B in the present calculations. Considering the fact that bands A and B are lying close to each other, band B might be a chiral partner band of band A.

To justify the chiral nature of bands A and B, the magnitude of triaxial deformation and the orientation angles θ and ϕ of the total angular momentum $\boldsymbol{J}$ in the intrinsic frame are examined. The obtained results are very similar its neighbouring odd-odd nucleus ^{106}Ag [53]. In Fig. 10(a), the potential energy surface of ^{104}Ag at the rotational frequency $\hbar\omega = 0.4$MeV is shown with the configuration fixed to $\alpha-$. Although the triaxial deformation is only $\gamma \approx 5^\circ$ at the minimum, the potential energy surface is soft in the triaxial direction; the energy rise is less than 1.5 MeV with the change in triaxial deformation of 22°. For the orientation angles of the total angular momentum $\boldsymbol{J}$ in the intrinsic frame, the polar angle θ varies from 64° to 80° driven by the increasing rotational frequency from 0.1 MeV to 0.6 MeV, while the azimuth angle ϕ vanishes at all rotational frequencies. Although this corresponds to a planar rotation, the angular momentum $\boldsymbol{J}$ can execute a quantal motion, oscillating around the planar equilibrium into the left- and right-handed sectors, which leads to the so-called chiral vibration. The experimental observation of chiral vibration requires a relatively low vibrational energy, which in turn requires a slow rise in Routhian curve along the ϕ degree of freedom. In Fig. 10 (b), the total Routhian curve at rotational frequency $\hbar\omega = 0.4$MeV for the configuration $\alpha-$ is shown as a function of the azimuth angle ϕ_ω of the angular velocity $\boldsymbol{\omega}$. It can be seen that the Routhian grows very slowly with the increasing ϕ_ω; rising only several tens of keV from $\phi_\omega = 0^\circ$ to 30°. This indicates that the chiral vibration around the planar equilibrium into

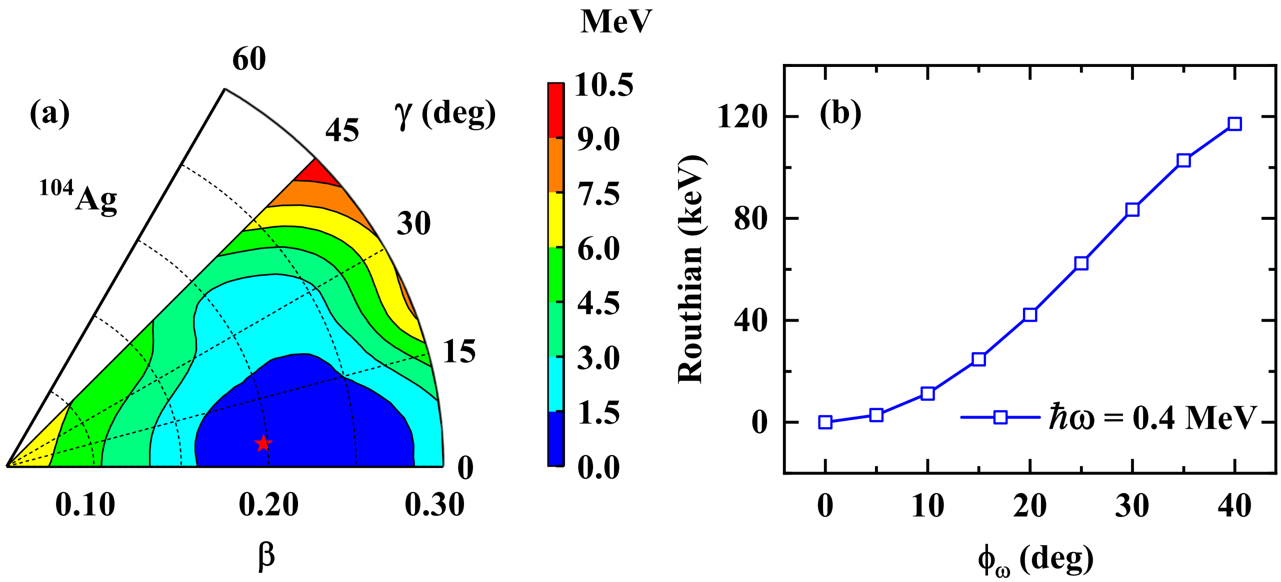

FIG. 10. Potential energy surface in the $\beta-\gamma$ deformation plane (left) and total Routhian curve as a function of the azimuth angle ϕ_ω of the angular velocity $\boldsymbol{\omega}$ (right) for the configuration $\pi g_{9/2}^{-1} \otimes \nu h_{11/2}(gd)^2$ at the rotational frequency $\hbar\omega = 0.4$MeV. The star denotes the position of the minimum energy in the potential energy surface. The Routhian curve is renormalized to its minima at $\phi_\omega = 0°$.

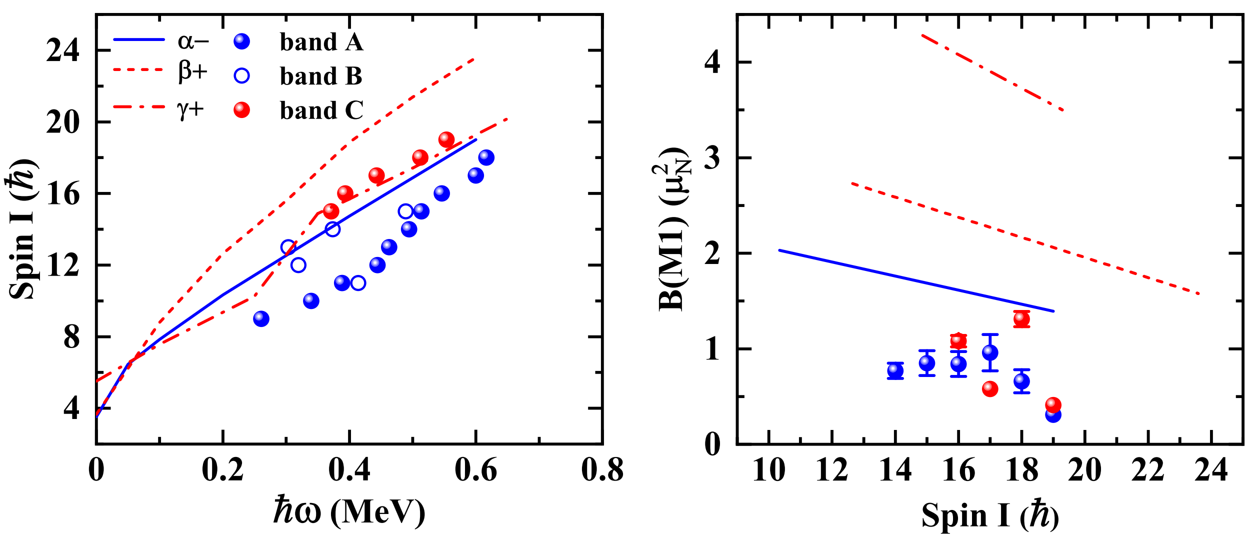

FIG. 11. The angular momentum as a function of rotational frequency and B(M1) as a function of spin for configurations $\alpha-, \beta+$ and $\gamma+$ in comparison with the data.

the left- and right-handed sectors should be substantial, and a pair of chiral vibrational bands can be generated based on the configuration $\alpha-$.

Amongst the positive-parity configurations, $\alpha+$ corresponds to the low-lying states with single-particle nature as suggested in Ref. [18]. Both configurations $\beta+$ and $\gamma+$ are possible for band C from the energy spectra and the final result needs the help from the angular momenta and $B(M1)$ results in Fig. 11.

The angular momentum vs. rotational frequency and $B(M1)$ vs. spin curves for configurations $\alpha-$, $\beta+$ and $\gamma+$ are also compared with the data as shown in Fig. 11. The calculated angular momenta and B(M1) values based on $\alpha-$ reproduce the data reasonably well, thus the configuration assignment to bands A and B is validated. For band C, the angular momenta and $B(M1)$ values are reproduced well based on the configuration $\beta+$. Even though the calculated angular momenta based

TABLE IV. Binding energies, deformations β and γ, and the corresponding configurations for the minima $\alpha+$, $\beta+$, $\gamma+$, $\alpha-$ and $\beta-$ in ^{104}Ag obtained in the configuration-fixed 3DTAC-CDFT calculations with PC-PK1.

State	E(MeV)	β	γ	Configurations
$\alpha+$	886.9	0.189	0.0°	$\pi(g_{9/2}^{-3}) \otimes \nu(g_{7/2}, d_{5/2})^7$
$\beta+$	883.7	0.240	7.5°	$\pi(g_{9/2}^{-3}) \otimes \nu(h_{11/2}^2)(g_{7/2}, d_{5/2})^5$
$\gamma+$	884.5	0.220	19.4°	$\pi(g_{9/2}^{-2})(p_{1/2}, p_{3/2})^{-1} \otimes \nu(h_{11/2}^1)(g_{7/2}, d_{5/2})^6$
$\alpha-$	885.7	0.220	0.0°	$\pi(g_{9/2}^{-3}) \otimes \nu(h_{11/2}^1)(g_{7/2}, d_{5/2})^6$
$\beta-$	883.4	0.242	39.0°	$\pi(g_{9/2}^{-1})(p_{1/2}, p_{3/2})^{-2} \otimes \nu(h_{11/2}^1)(g_{7/2}, d_{5/2})^6$

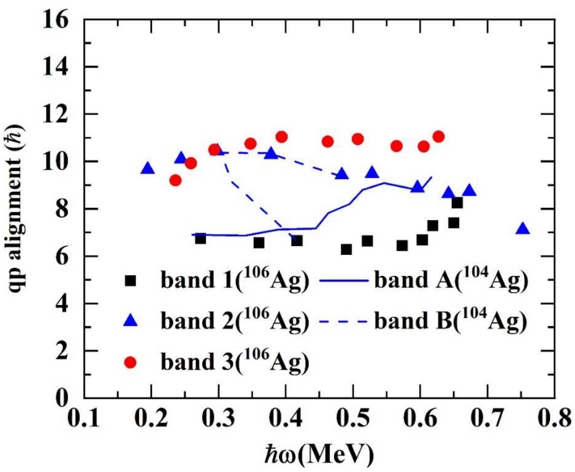

FIG. 12. Plot of the quasiparticle alignment as a function of spin for ^{104}Ag and ^{106}Ag. The Harries parameters used are $\Im_0$=7.0 $\hbar^2$/MeV, $\Im_1$=15.0 $\hbar^4$/MeV [46].

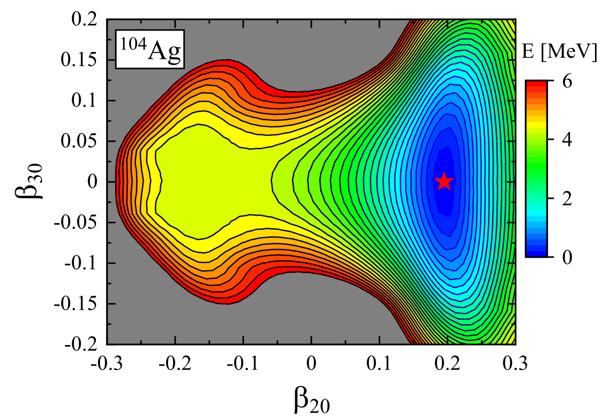

FIG. 13. The potential energy surface of ^{104}Ag calculated using 3D lattice CDFT. The energies are normalized to the ground state with $(\beta_{20}, \beta_{30}) = (0.195, 0.0)$. The contour separation is 0.2 MeV.

on $\gamma+$ reproduce the data satisfactorily, $\gamma+$ should be excluded because it strongly overestimates the $B(M1)$ values. The theoretically suggested configuration is consistent with the one suggested in Ref. [19], however, the deformation parameters predicted from present calculations are β=0.24 and γ=7.5^o while in Ref. [19] it was suggested to be β=0.18 and γ=25^o.

The quasiparticle alignments of bands A and B can be compared with those of bands 1-3 from the neighbouring odd-odd nucleus ^{106}Ag [17, 53] as shown in Fig. 12. The configuration of band A can be assigned as $\pi g_{9/2}^{-1} \otimes \nu h_{11/2}$ at low spins and as $\pi g_{9/2}^{-1} \otimes \nu h_{11/2}(gd)^2$ at high spins. The configuration of band B can be assigned as $\pi g_{9/2}^{-1} \otimes \nu h_{11/2}(gd)^2$. Bands A and B are probably chiral doublet bands based on $\pi g_{9/2}^{-1} \otimes \nu h_{11/2}(gd)^2$, similar to the bands 2 and 3 in ^{106}Ag.

Experimentally, there are a few relatively strong E1 transitions connecting the positive-parity band and the yrast negative-parity band. To explore the octupole correlations in ^{104}Ag, the potential energy surface in the $\beta_{20} - \beta_{30}$ plane for the ground state of ^{104}Ag is calculated by CDFT in 3D lattice and shown in Fig. 13. For the CDFT calculations, the step sizes along the x, y and z axes are chosen as 1.0 fm. The grid numbers are 24 for the x and y axes and 28 for the z axis. The size of the space adopted here is sufficient to obtain converged solutions. Although the octupole deformation $\beta_{30} = 0°$ at the minimum, the potential energy surface is rather soft in the octupole direction; the energy rise is less than 0.4 MeV with change in octupole deformation of 0.05. Similar to the interpretation for the chiral doublet bands with octupole correlations in ^{124}Cs [37] and ^{78}Br [66], the octupole soft nature predicted in ^{104}Ag is expected to be responsible for the enhanced $E1$ transitions between the positive and negative-parity bands.

V. SUMMARY

High spin structure in ^{104}Ag nucleus has been investigated through the fusion evaporation reaction ^{76}Ge(^{32}S, p3n) at beam energy of 110 MeV. In the present study, lifetime measurements have been done for various states in the negative-parity yrast band and positive-parity magnetic rotational band at an excitation energy of 4424 keV. Lifetimes of 7 states and upper limits on lifetime of 3 states were obtained using the DSAM technique. Lifetime of 3 states (17^-, 18^-, 19^-) of yrast band and 16^+ state of positive band based on 4424 keV have been determined for the first time. In case of states where lifetime have been known from earlier studies, the errors have been reduced significantly. From our directional correlation measurements of gamma rays (DCO) we have also been able to confirm some of the spin-parity assignments which were tentatively assigned before. We have observed enhanced E1 transitions (three known from earlier studies and two more from the present study) from the positive-parity band based on 4424 keV to the yrast and its proposed (from earlier study) chiral partner band. We have performed calculations based on TPSM and CDFT approaches to understand the above mentioned band structures. It is evident from the presented results that TPSM provides a reasonable description of all the properties of the two observed negative-parity bands. Further, it has been shown that two bands have finite angular-momentum projections along the three principle axis, which indicates that two bands could be associated with the chiral symmetry breaking. The CDFT calculations suggest assignment of $\pi g_{9/2}{}^{-1} \otimes \nu h_{11/2}$ for the yrast band and above spin of $\sim 12\hbar$, $\pi(g_{9/2})^{-1} \otimes \nu(h_{11/2})(g_{7/2},d_{5/2})^2$ aligned quasiparticle configuration for the yrast and the partner band. The deformations predicted for the yrast and the partner band are $\beta \approx 0.20$ and $\gamma \approx 5^o$ at higher spins. The partner band can be thought to be a chiral vibrational mode built on top of the yrast band. The positive-parity band based on 4424 keV state is predicted to have $\pi(g_{9/2})^{-1} \otimes \nu(h_{11/2})^2(g_{7/2},d_{5/2})^1$ aligned quasiparticle configuration. The potential energy surface calculations based on CDFT predicts significant softness with respect to octupole deformation and this could be the reason for the enhanced E1 transitions from the above positive-parity band to the yrast and it's chiral partner band. This is analogous to the octupole correlations observed along with chiral doublet bands in ^{78}Br and ^{124}Cs.

ACKNOWLEDGEMENT

We would like to acknowledge BARC-TIFR pelletron staff for delivering a stable beam of ^{32}S during the experiment. We acknowledge the help of all INGA collaboration. Authors gratefully to Department of Science and Technology (DST) for INGA project (No.IR/S2/PF-30/2003-II). This work was supported by the Department of Atomic Energy, Government of India (Project Identification No. RTI 4002). One of the author K.K. acknowledges CSIR (09/760(0032)/2017-EMR-I) for financial support as research grant. This work was supported by the National Science Foundation (Grant No. PHY-1068192 and PHY-2011890) and by the APS-IUSSTF Physics Student and Post-doc Visitation Program. The authors S. Jehangir, G. H. Bhat, N. Rather and J. A. Sheikh like to acknowledge Science and Engineering Research Board (SERB), Department of Science and Technology (Government of India) for providing financial assistance under the Project No.CRG/2019/004960 to carry out a part of the present research work. We would also like to thank R. Bhattacharjee, S. S. Bhattacharjee, S. Samanta, S. Das, N. Ghosh, A. K. Sinha, S. Mukhopadhyay, L. Dhanu, B. K. Nayak, D. C. Biswas, A. Y. Deo, S. K. Tandel, N. Kaur, Ashok Kumar, J. Sethi and S. Chattopadhyay for their initial involvement in the project. Fruitful discussion with J. Meng and Z. X. Ren on the theoretical interpretation are also acknowledged. A special thanks to Prof. S. C. Pancholi for his unconditional guidance.

---

[1] S. Frauendorf, Nucl. Phys. A **557**, 259 (1993).

[2] R. M. Clark and A. O. Macchiavelli, Annual Review of Nuclear and Particle Science **50**, 1 (2000).

[3] H. Hubel, Progress in Particle and Nuclear Physics **54**, 1 (2005).

[4] S. Frauendorf, Reviews of Modern Physics **73**, 463 (2001).

[5] S. Frauendorf and J. Meng, Nucl. Phys. A **617**, 131 (1997).

[6] P. Joshi, D. G. Jenkins, P. M. Raddon, A. J. Simons, R. Wadsworth, A. R. Wilkinson, D. B. Fossan, T. Koike, K. Starosta, C. Vaman, J. Timár, Z. Dombrádi, A. Krasznahorkay, J. Molnár, D. Sohler, L. Zolnai, A. Algora, E. S. Paul, G. Rainovski, A. Gizon, J. Gizon, P. Bednarczyk, D. Curien, G. Duchêne, and J. N. Scheurer, Phys. Lett B. **595**, 135 (2004).

[7] C. Vaman, D. B. Fossan, T. Koike, K. Starosta, I. Y. Lee, and A. O. Macchiavelli, Phys. Rev. Lett **92**, 032501 (2004).

[8] T. Suzuki, G. Rainovski, T. Koike, T. Ahn, M. P. Carpenter, A. Costin, M. Danchev, A. Dewald, R. V. F. Janssens, P. Joshi, C. J. Lister, O. Möller, N. Pietralla, T. Shinozuka, J. Timár, R. Wadsworth, C. Vaman, and S. Zhu, Phys. Rev. C **78**, 031302(R) (2008).

[9] J. Timar, C. Vaman, K. Starosta, D. B. Fossan, T. Koike, D. Sohler, I. Y. Lee, and A. O. Macchiavelli, Phys. Rev. C **73**, 011301(R) (2006).

[10] P. Joshi, M. P. Carpenter, D. B. Fossan, T. Koike, E. S. Paul, G. Rainovski, K. Starosta, C. Vaman, and R. Wadsworth, Phys. Rev. Lett **98**, 102501 (2007).

[11] T. Koike, K. Starosta, C. J. Chiara, D. B. Fossan, and D. R. LaFosse, Phys. Rev. C **67**, 044319 (2003).

[12] W. Shou-Yu, Z. Shuang-Quan, Q. Bin, and M. Jie, Chinese Phys. Lett. **24**, 664 (2007).

[13] D. Tonev, G. de Angelis, S. Brant, S. Frauendorf, P. Petkov, A. Dewald, F. Dönau, D. L. Balabanski, Q. Zhong, P. Pejovic, D. Bazzacco, P. Bednarczyk, F. Camera, D. Curien, F. D. Vedova, A. Fitzler, A. Gadea, G. L. Bianco, S. Lenzi, S. Lunardi,

N. Marginean, O. Möller, D. R. Napoli, R. Orlandi, E. Sahin, A. Saltarelli, J. V. Dobon, K. O. Zell, J. ye Zhang, and Y. H. Zhang, Phys. Rev. C **76**, 044313 (2007).

[14] D. Tonev, M. Yavahchova, N. Goutev, G. de Angelis, P. Petkov, R. Bhowmik, R. Singh, S. Muralithar, N. Madhavan, R. Kumar, M. K. Raju, J. Kaur, G. Mohanto, A. Singh, N. Kaur, R. Garg, A. Shukla, T. Marinov, and S. Brant, Phys. Rev. Lett **112**, 052501 (2014).

[15] E. Grodner, I. Sankowska, T. Morek, S. G. Rohoziński, C. Droste, J. Srebrny, A. A. Pasternak, M. Kisieliński, M. Kowalczyk, J. Kownacki, J. Mierzejewski, A. Król, and K. Wrzosek, Phys. Lett. B **703**, 46 (2011).

[16] E. Grodner, J. Srebrny, A. A. Pasternak, I. Zalewska, T. Morek, C. Droste, J. Mierzejewski, M. Kowalczyk, J. Kownacki, M. Kisieliński, S. G. Rohoziński, T. Koike, K. Starosta, A. Kordyasz, P. J. Napiorkowski, M. Wolińska-Cichocka, E. Ruchowska, W. Płóciennik, and J. Perkowski, Phys. Rev. Lett **97**, 172501 (2006).

[17] E. Lieder, R. Lieder, R. Bark, Q. Chen, S. Zhang, J. Meng, E. Lawrie, J. Lawrie, S. Bvumbi, N. Kheswa, S. Ntshangase, T. Madiba, P. Masiteng, S. Mullins, S. Murray, P. Papka, D. Roux, O. Shirinda, Z. Zhang, P. Zhao, Z. Li, J. Peng, B. Qi, S. Wang, Z. Xiao, and C. Xu, Phys. Rev. Lett **112**, 202502 (2014).

[18] Z. G. Wang, M. L. Liu, Y. H. Zhang, X. H. Zhou, B. T. Hu, N. T. Zhang, S. Guo, B. Ding, Y. D. Fang, J. G. Wang, G. S. Li, Y. H. Qiang, S. C. Li, B. S. Gao, Y. Zheng, W. Hua, X. G. Wu, C. Y. He, Y. Zheng, C. B. Li, J. J. Liu, and S. P. Hu, Phys. Rev. C **88**, 024306 (2013).

[19] P. Datta, S. Chattopadhyay, P. Banerjee, S. Bhattacharya, B. Dasmahapatra, T. K. Ghosh, A. Goswami, S. Pal, M. S. Sarkar, S. Sen, H. C. Jain, P. K. Joshi, and Amita, Phys. Rev. C **69**, 044317 (2003).

[20] W. A. Dar, J. A. Sheikh, G. H. Bhat, R. Palit, R. N. Ali, and S. Frauendorf, Nucl. Phys. A **933**, 123 (2015).

[21] R. Palit, S. Saha, J. Sethi, T. Trivedi, S. Sharma, B. S. Naidu, S. Jadhav, R. Donthi, P. B. Chavan, H. Tan, and W. Hennig, Nuclear Instruments and Methods in Physics Research A **680**, 90 (2012).

[22] D. C. Radford, Nuclear Instruments and Methods in Physics Research A **361**, 297 (1995).

[23] D. C. Radford, Nuclear Instruments and Methods in Physics Research A **361**, 306 (1995).

[24] K. S. Krane, R. M. Steffen, and R. M. Wheeler, Atomic Data and Nuclear Data Tables **11**, 351 (1973).

[25] J. Tréherne, J. Genevey, S. André, R. Béraud, A. Charvet, R. Duffait, A. Emsallem, M. Meyer, C. Bourgeois, P. Kilcher, J. Sauvage, F. A. Beck, and T. Byrski, Phys. Rev. C **27**, 166 (1983).

[26] J. C. Wells and N. R. Johnson, Report No. ORNL-6689, 44 (1991).

[27] S. Das, S. Samanta, R. Bhattacharjee, R. Raut, S. S. Ghugre, A. K. Sinha, U. Garg, R. Chakrabarti, S. Mukhopadhyay, A. Dhal, M. K. Raju, N. Madhavan, S. Muralithar, R. P. Singh, K. Suryanarayana, P. V. M. Rao, R. Palit, S. Saha, and J. Sethi, Nucl. Phys. A **841**, 17 (2017).

[28] www.srim.org.

[29] A. Sharma, R. Raut, S. Muralithar, R. P. Singh, S. S. Bhattacharjee, S. Das, S. Samanta, S. S. Ghugre, R. Palit, S. Jehangir, N. Rather, G. H. Bhat, J. A. Sheikh, S. S. Tiwary, Neelam, P. V. M. Rao, U. Garg, and S. K. Dhiman, Phys. Rev. C **103**, 044322 (2021).

[30] T. K. Alexander and J. S. Forster, Advances in Nuclear Physics **10**, 197 (1978).

[31] C. Y. He, L. H. Zhu, X. G. Wu, S. X. Wen, G. S. Li, Y. Liu, Z. M. Wang, X. Q. Li, X. Z. Cui, H. B. Sun, R. G. Ma, and C. X. Yang, Phys. Rev. C **81**, 057301 (2010).

[32] C. Liu, S. Y. Wang, B. Qi, D. P. Sun, C. J. Xu, L. Liu, B. Wang, X. C. Shen, M. R. Qin, H. Chen, L. H. Zhu, X. G. Wu, G. S. Li, C. Y. He, Y. Zheng, L. L. Wang, B. Zhang, G. Y. Liu, and Y. W. Wang, Int. J. Mod. Phys. E **20**, 2351 (2011).

[33] G. de Angelis, C. Fahlander, A. Gadea, E. Farnea, D. Bazzacco, N. Belcari, N. Blasi, P. G. Bizzeti, A. Bizzeti-Sona, D. de Acuña, M. D. Poli, H. Grawe, A. Johnson, G. L. Bianco, S. Lunardi, D. R. Napoli, J. Nyberg, P. Pavan, J. Persson, C. R. Alvarez, D. Rudolph, R. Schubart, P. Spolaore, R. Wyss, and F. Xu, Phys. Lett. B **437**, 236 (1998).

[34] G. J. Lane, D. B. Fossan, J. M. Sears, J. F. Smith, J. A. Cameron, R. M. Clark, I. M. Hibbert, V. P. Janzen, R. Krucken, I. Y. Lee, A. O. Macchiavelli, and C. M. Parry, Phys. Rev. C **57**, R1022 (1998).

[35] G. de Angelis, A. Gadea, E. Farnea, R. Isocrate, P. Petkov, N. Marginean, D. R. Napoli, A. Dewald, M. Bellato, A. Bracco, F. Camera, D. Curien, M. De Poli, E. Fioretto, A. Fitzler, S. Kasemann, N. Kintz, T. Klug, S. Lenzi, S. Lunardi, R. Menegazzo, P. Pavan, J. L. Pedroza, V. Pucknell, C. Ring, J. Sampson, and R. Wyss, Phys. Lett. B **535**, 93 (2002).

[36] Z. Liu, X. Sun, X. Zhou, X. Lei, Y. Guo, Y. Zhang, X. Chen, H. Jin, Y. Luo, S. X. Wen, C. X. Yang, G. J. Yuan, G. S. Li, X. A. Liu, W. D. Luo, and Y. S. Chen, Eur. Phys. J. A. **1**, 125 (1998).

[37] K. Selvakumar, A. K. Singh, C. Ghosh, P. Singh, A. Goswami, R. Raut, A. Mukherjee, U. Datta, P. Datta, S. Roy, G. Gangopadhyay, S. Bhowal, S. Muralithar, R. Kumar, R. P. Singh, and M. K. Raju, Phys. Rev. C **92**, 064307 (2015).

[38] P. Mason, G. Benzoni, A. Bracco, F. Camera, B. Million, O. Wieland, S. Leoni, A. K. Singh, A. A. Khatib, H. Hubel, P. Bringel, A. Burger, A. Neusser, G. Schonwasser, B. M. Nyako, J. Timar, A. Algora, Z. Dombradi, J. Gal, G. Kalinka, J. Molnar, D. Sohler, L. Zolnai, K. Juhasz, G. B. Hagemann, C. R. Hansen, B. Herskind, G. Sletten, M. Kmiecik, A. Maj, J. Styczen, K. Zuber, F. Azaiez, K. Hauschild, A. Korichi, A. Lopez-Martens, J. Roccaz, S. Siem, F. Hannachi, J. N. Scheurer, P. Bednarczyk, T. Byrski, D. Curien, O. Dorvaux, G. Duchene, B. Gall, F. Khalfallah, I. Piqueras, J. Robin, S. B. Patel, O. A. Evans, G. Rainovski, C. M. Petrache, D. Petrache, G. L. Rana, R. Moro, G. D. Angelis, P. Fallon, I. Y. Lee, J. C. Lisle, B. Cederwall, K. Lagergen, R. M. Lieder, E. Podsvirova, W. Gast, H. Jager, N. Redon, and A. Gorgen, Phys. Rev. C **72**, 064315 (2005).

[39] J. A. Sheikh, G. H. Bhat, W. A. Dar, S. Jehangir, and P. A. Ganai, Phys.Scr. **91**, 063015 (2016).

[40] S. Jehangir, G. H. Bhat, N. Rather, J. A. Sheikh, and R. Palit, Phys. Rev. C **104**, 044322 (2021).

[41] S. Jehangir, I. Maqbool, G. H. Bhat, J. A. Sheikh, R. Palit, and N. Rather, Eur. Phys. J. A **56**, 197 (2020).

[42] G. H. Bhat, J. A. Sheikh, W. A. Dar, S. Jehangir, R. Palit, and P. A. Ganai, Phys. Lett. B **738**, 218 (2014).

[43] G. H. Bhat, J. A. Sheikh, and R. Palit, Phys. Lett. B **707**, 250 (2012).

[44] P. Moller, J. R. Nix, W. D. Myers, and W. J. Swiatecki, Atomic Data and Nuclear Data Tables **59**, 185 (1995).

[45] P. S. Peter Ring, Springer Berlin Heidelberg (1980).

[46] P. H. Regan, A. E. Stuchbery, G. D. Dracoulis, A. P. Byrne, G. J. Lane, T. Kibédi, D. C. Radford, A. Galindo-Uribarri, V. P. Janzen, D. Ward, S. M. Mullins, G. Hackman, J. H. DeGraaf, M. Cromaz, and S. Pilotte, Nucl. Phys. A **586**, 351 (1995).

[47] D. A. Volkov, A. I. Kovalenko, A. I. Levon, A. S. Mishin, A. A. Pas-ternak, and L. A. Rassadin, Izv. Akad. Nauk SSSR Ser. Fiz.Izv. Akad. Nauk SSSR Ser. Fiz. **53**, 923 (1989).

[48] B. M. Musangu, E. H. Wang, J. H. Hamilton, S. Jehangir, G. H. Bhat, J. A. Sheikh, S. Frauendorf, C. J. Zachary, J. M. Eldridge, A. V. Ramayya, A. C. Dai, F. R. Xu, J. O. Rasmussen, Y. X. Luo, G. M. Ter-Akopian, Y. T. Oganessian, and S. J. Zhu, Phys. Rev. C **104**, 064318 (2021).

[49] P. Ring, Progress in Particle and Nuclear Physics **37**, 193 (1996).

[50] J. Meng, ed., Relativistic Density Functional for Nuclear Structure, International Review of Nuclear Physics, Vol. 10 (World Scientific, Singapore, 2016).

[51] J. Meng and P. Zhao, AAPPS **31**, 2 (2021).

[52] P. W. Zhao, Phys. Lett. B **773**, 1 (2017).

[53] P. W. Zhao, Y. K. Wang, and Q. B. Chen, Phys. Rev. C **99**, 054319 (2019).

[54] C. M. Petrache, B. F. Lv, A. Astier, E. Dupont, Y. K. Wang, S. Q. Zhang, P. W. Zhao, Z. X. Ren, J. Meng, P. T. Greenlees, H. Badran, D. M. Cox, T. Grahn, R. Julin, S. Juutinen, J. Konki, J. Pakarinen, P. Papadakis, J. Partanen, P. Rahkila, M. Sandzelius, J. Saren, C. Scholey, J. Sorri, S. Stolze, J. Uusitalo, B. Cederwall, O. Aktas, A. Ertoprak, H. Liu, S. Matta, P. Subramaniam, S. Guo, M. L. Liu, X. H. Zhou, K. L. Wang, I. Kuti, J. Timar, A. Tucholski, J. Srebrny, and C. Andreoiu, Phys. Rev. C **97**, 041304(R) (2018).

[55] Z. X. Ren, S. Q. Zhang, and J. Meng, Phys. Rev. C **95**, 024313 (2017).

[56] Z. Ren, S. Zhang, P. Zhao, N. Itagaki, J. A. Maruhn, and J. Meng, China Physics, Machenics and Astronomy **62**, 112062 (2019).

[57] Z. X. Ren, P. W. Zhao, S. Q. Zhang, and J. Meng, Nucl. Phys. A **996**, 121696 (2020).

[58] P. W. Zhao, Z. P. Li, J. M. Yao, and J. Meng, Phys. Rev. C **82**, 054319 (2010).

[59] K. Zhang, M.-K. Cheoun, Y.-B. Choi, P. S. Chong, J. Dong, L. Geng, E. Ha, X. He, C. Heo, M. C. Ho, E. J. In, S. Kim, Y. Kim, C.-H. Lee, J. Lee, Z. Li, T. Luo, J. Meng, M.-H. Mun, Z. Niu, C. Pan, P. Papakonstantinou, X. Shang, C. Shen, G. Shen, W. Sun, X.-X. Sun, C. K. Tam, Thaivayongnou, C. Wang, S. H. Wong, X. Xia, Y. Yan, R. W. Y. Yeung, T. C. Yiu, S. Zhang, W. Zhang, and S. G. Zhou, Phys. Rev. C **102**, 024314 (2020).

[60] Y. L. Yang, Y. K. Wang, P. W. Zhao, and Z. P. Li, Phys. Rev. C **104**, 054312 (2021).

[61] K. Zhang, M.-K. Cheoun, Y.-B. Choi, P. S. Chong, J. Dong, Z. Dong, X. Du, L. Geng, E. Ha, X.-T. He, C. Heo, M. C. Ho, E. J. In, S. Kim, Y. Kim, C.-H. Lee, J. Lee, H. Li, Z. Li, T. Luo, J. Meng, M.-H. Mun, Z. Niu, C. Pan, P. Papakonstantinou, X. Shang, C. Shen, G. Shen, W. Sun, X.-X. Sun, C. K. Tam, Thaivayongnou, C. Wang, X. Wang, S. H. Wong, J. Wu, X. Wu, X. Xia, Y. Yan, R. W.-Y. Yeung, T. C. Yiu, S. Zhang, W. Zhang, X. Zhang, Q. Zhao, and S. G. Zhou, Atomic Data and Nuclear Data Tables **144**, 101488 (2022).

[62] P. W. Zhao, J. Peng, H. Z. Liang, P. Ring, and J. Meng, Phys. Rev. Lett **107**, 122501 (2011).

[63] P. W. Zhao, S. Q. Zhang, J. Peng, H. Z. Liang, P. Ring, and J. Meng, Phys. Lett. B **699**, 181 (2011).

[64] J. Meng and P. Zhao, Phys. Scr. **91**, 053008 (2016).

[65] J. Meng, J. Peng, S. Q. Zhang, and S.-G. Zhou, Phys. Rev. C **73**, 037303 (2006).

[66] C. Liu, S. Wang, R. Bark, S. Zhang, J. Meng, B. Qi, P. Jones, S. Wyngaardt, J. Zhao, C. Xu, S.-G. Zhou, S. Wang, D. Sun, L. Liu, Z. Li, N. Zhang, H. Jia, X. Li, H. Hua, Q. Chen, Z. Xiao, H. Li, L. Zhu, T. Bucher, T. Dinoko, J. Easton, K. Juhász, A. Kamblawe, E. Khaleel, N. Khumalo, E. Lawrie, J. Lawrie, S. Majola, S. Mullins, S. Murray, J. Ndayishimye, D. Negi, S. Noncolela, S. Ntshangase, B. Nyakó, J. Orce, P. Papka, J. Sharpey-Schafer, O. Shirinda, P. Sithole, M. Stankiewicz, and M. Wiedeking, Phys. Rev. Lett **116**, 112501 (2016).